Site-Selective Deposition of Twinned Platinum Nanoparticles on $TiSi_2$ Nanonets by Atomic Layer Deposition and Their Oxygen Reduction Activities

Jin Xie,[†,‡] Xiaogang Yang,[†,‡] Binghong Han,[§] Yang Shao-Horn,[§] and Dunwei Wang[†,*]

[†]Department of Chemistry, Merkert Chemistry Center, Boston College, Chestnut Hill, Massachusetts 02467, United States, and [§]Department of Mechanical Engineering and Department of Materials Science and Engineering, Massachusetts Institute of Technology, Cambridge, Massachusetts 02139, United States. [‡]J. Xie and X. Yang contributed equally.

ABSTRACT For many electrochemical reactions such as oxygen reduction, catalysts are of critical importance, as they are often necessary to reduce reaction overpotentials. To fulfill the promises held by catalysts, a well-defined charge transport pathway is indispensable. Presently, porous carbon is most commonly used for this purpose, the application of which has been recently recognized to be a potential source of concern. To meet this challenge, here we present the development of a catalyst system without the need for carbon. Instead, we focused on a conductive, two-dimensional material of a $TiSi_2$ nanonet, which is also of high surface area. As a proof-of-concept, we grew Pt nanoparticles onto $TiSi_2$ by atomic layer deposition. Surprisingly, the growth exhibited a unique selectivity, with Pt deposited only on the top/bottom surfaces of the nanonets at the nanoscale without mask or patterning. Pt {111} surfaces are preferably exposed as a result of a multiple-twinning effect. The materials showed great promise in catalyzing oxygen reduction reactions, which is one of the key challenges in both fuel cells and metal air batteries.

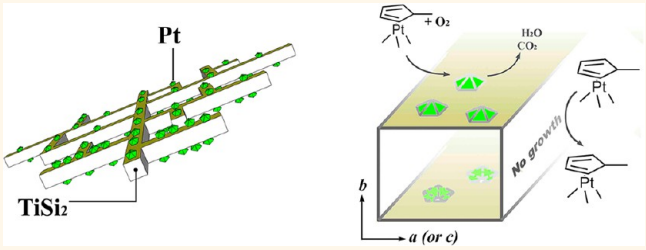

KEYWORDS: atomic layer deposition · oxygen reduction reaction · catalyst · platinum · nanonets · titanium disilicide

The discovery of materials with new compositions or novel morphologies or both has played an important role in advancing modern technologies such as those for electrical energy storage applications.[1−3] Conversely, the key challenges encountered in the development of these technologies are often connected to the material design, particularly that at the nanoscale. To illustrate this point, let us consider issues related to electrode design for proton exchange membrane fuel cells as an example.[4−8] To afford high current density, conductive frameworks with high surface area are desired for the electrode's construction. Porous carbon, especially those with nanoscale pores, is popularly used as a scaffold, onto which catalysts for ORR (oxygen reduction reaction) and/or HOR (hydrogen oxidation reaction) are dispersed. It has been realized that the choice of porous carbon presents issues that may limit the performance of fuel cells, including poor stability and reduced catalytic activities.[9] Indeed, poorer activities of ORR catalysts have been observed on a carbon support than on metal or metal alloy electrodes,[10−12] although in these examples carbon additives were still used to provide electrical transport pathways. To enable significant advances in the field of electrical energy storage, it is important to develop a conductive, porous material that is carbon free. On a fundamental level, this material may enable mechanistic studies to help understand what role a carbon support plays in degrading the performance of fuel cell electrodes. On a practical level, the new material may serve as a replacement for carbon in future devices. To date, examples of low-cost, non-carbon-based porous conductive frameworks remain rare other than those involving precious metals.[13,14]

* Address correspondence to dunwei.wang@bc.edu.

Received for review May 11, 2013 and accepted June 24, 2013.

Published online June 24, 2013
10.1021/nn402385f

Here we examine whether $TiSi_2$ nanonets, which are inexpensive in nature and easy to prepare,[15−17] are suitable for this purpose. Intriguingly, when used to grow Pt, a highly unusual selective deposition was obtained, resulting in 5-fold twinned Pt nanoparticles whose {111} planes are preferably exposed. The Pt/$TiSi_2$ combination exhibits ORR activities in aqueous solutions comparable to that of an optimized commercial Pt/C catalyst, establishing that the nanonet is in fact a promising candidate for air electrode design and construction.

For this proof-of-concept work, we chose to interface Pt with $TiSi_2$ because it is a well-known ORR catalyst in aqueous systems.[18,19] The wealth of prior knowledge about Pt catalytic behavior makes it easy to compare the performance of the Pt/$TiSi_2$ nanonet combination with that based on Pt/C. To obtain uniform coverage of Pt nanoparticles on the surface of $TiSi_2$ nanonets, which is important for electrochemical ORR reactions, atomic layer deposition (ALD) was used as the preparation method.[20] To our surprise and delight, a highly selective deposition was obtained, with Pt nanoparticles growing only on the (020) planes of $TiSi_2$ nanonets (see schematic illustration in Figure 1). Transmission electron micrographs (TEM) of top and side views (Figure 2a and b, respectively) confirmed that the deposition was indeed only on the top and bottom, but not on the side surfaces of $TiSi_2$ nanonets. For a total of more than 200 samples out of 30 batches of growth studied, all of them exhibited the same selectivity, thereby ruling out that the observation was a phenomenological effect. Although selective growth of nanoparticles such as Ag and Pt on the tips of ZnO[21] and CdS nanorods,[22,23] respectively, has been reported, similar selectivity of gas-phase-deposited nanoparticles on a nanostructured substrate has not been observed previously, to the best of our knowledge. We are therefore intrigued to study the possible causes for this unusual phenomenon.

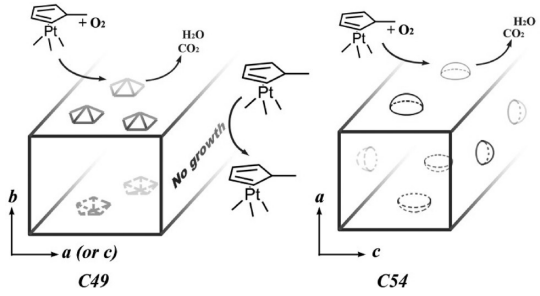

Figure 1. Schematics of Pt nanoparticle deposition on different $TiSi_2$ nanostructures. (Left) Selective deposition is achieved on the layered C49 $TiSi_2$, whose *b* planes consist of alternate layers of a Ti−Si mixture and Si-only atoms. Because the unit cell of C49 $TiSi_2$ is highly anisotropic (with a *b* lattice nearly four times that of *a* and *c*), its bulk form was known as metastable, and the only stable C49 $TiSi_2$ was found in nanonet morphology.[15,16] Pt nanoparticles grow on the top and bottom surfaces, which are the *b* planes terminated by Si. For clarity, only one beam is shown here. (Right) Pt nanoparticles grow nonselectively on all surfaces on C54 $TiSi_2$ nanowires that are identical in composition and similar in size to the nanonets. The main difference of C54 $TiSi_2$ from the C49 one is the lack of Si-only layers on its surface and, hence, the lack of layered, anisotropic structures.

RESULTS AND DISCUSSION

Different from its bulk and nanowire counterparts, the nanonet form of $TiSi_2$ is of a layered structure known as C49. Our previous research revealed that the top and bottom surfaces of $TiSi_2$ nanonets are the *b* planes, which are made of only Si atoms.[15] We hypothesize that the unique crystal structure is the key reason for the selective deposition as described above. To prove the growth is indeed specific to $TiSi_2$ nanonets, the following control experiments were carried out. First, Pt deposition on $TiSi_2$ nanowires was studied. As shown in Figure 1b schematically, and in Figure 3a and b, Pt nanoparticles of sizes comparable to those grown on $TiSi_2$ nanonets were obtained, but without obvious selectivity in their deposition sites, meaning that Pt nanoparticles were evenly distributed on all surfaces of the $TiSi_2$ nanowires. Given that $TiSi_2$ nanowires

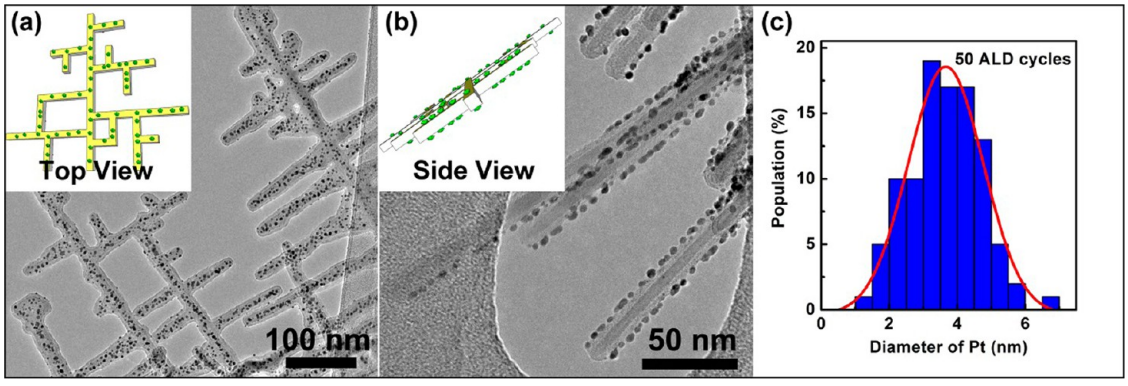

Figure 2. Microstructures of Pt/$TiSi_2$ heteronanostructures by a typical 50-cycle ALD growth. (a) When viewed from the top, a uniform distribution of Pt nanoparticles is observed. (b) When viewed from the side, Pt nanoparticles are seen only on the top and bottom surfaces of $TiSi_2$. The relationship is schematically illustrated in the insets. (c) The size distribution of Pt nanoparticles.

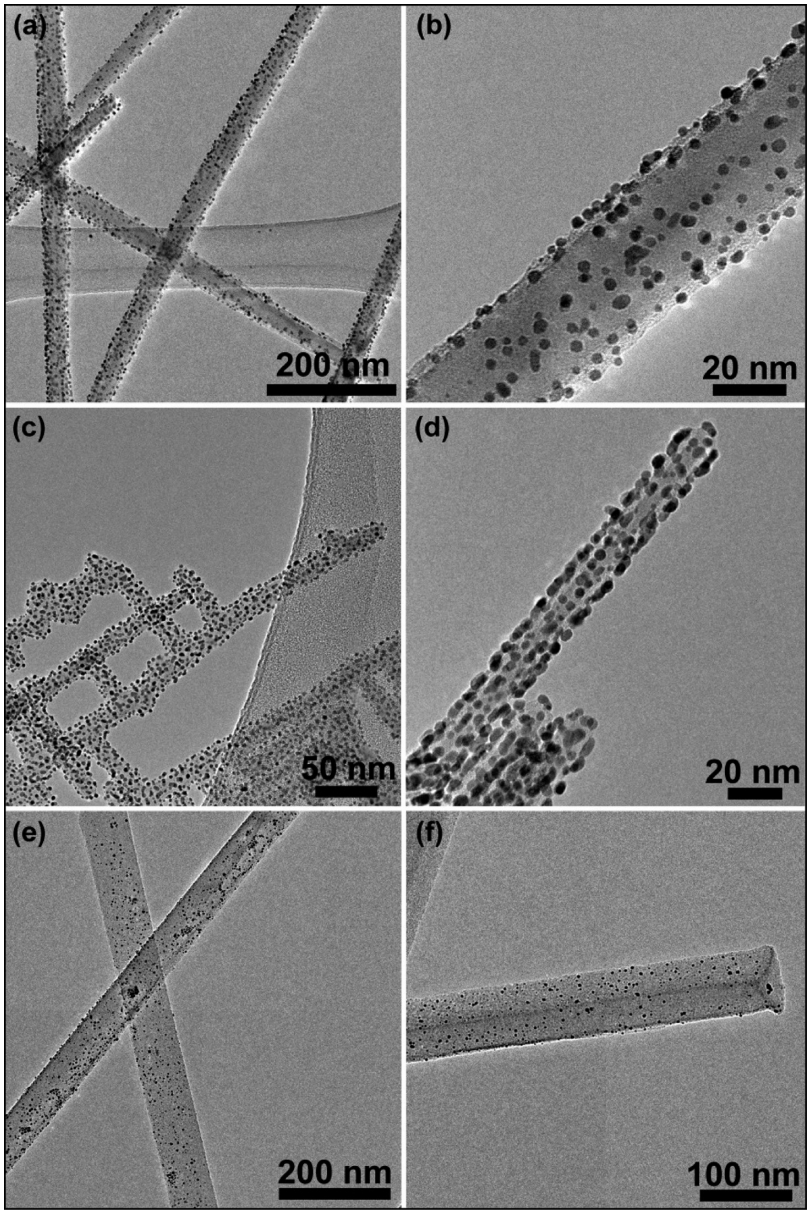

Figure 3. Transmission electron micrographs of Pt nanoparticles on various substrates by the ALD method. (a, b) C54 $TiSi_2$ nanowires; (c, d) TiO_2-coated C49 $TiSi_2$ nanonets; (e, f) Si nanowires.

are of similar sizes and identical chemical compositions to $TiSi_2$ nanonets, it is understood that the small sizes (*ca.* ~20 nm in diameters) and chemical compositions ($TiSi_2$) are not the causes for the selective deposition. Second, to understand whether the nanonet morphology played a role in the selective deposition, we first grew a thin layer (10 ALD cycles) of TiO_2 by ALD on $TiSi_2$ nanonets, converting the surfaces (top, bottom, and sides) to a nondistinguishable TiO_2 coverage.[24] Subsequent ALD growth resulted in a uniform deposition of Pt nanoparticles (in Figure 3c and d). This result suggests the morphology alone is not the reason for the selective growth. Taken as a whole, we concluded that the selective deposition of Pt nanoparticles was specific to $TiSi_2$ nanonets, and the surfaces are the key reason for the selectivity. For the completeness of discussions about the uniqueness of $TiSi_2$ nanonets and important to electrocatalytic applications, it is worth noting that $TiSi_2$ nanonets exhibit a resistivity of *ca.* ~10 $\mu\Omega$ cm, which is approximately 10 times better than bulk C49 $TiSi_2$ and comparable to the more conductive C54. Our earlier work suggests that the improved conductivity is due to the lack of stacking faults along the *b* direction in the nanonets.[15]

Previous research suggests that ALD growth of Pt with trimethyl(methylcyclopentadienyl) platinum(IV) ($MeCpPtMe_3$) as a precursor starts with chemisorption of $MeCpPtMe_2$, followed by oxidation of the remaining ligands to yield elemental Pt.[20] When the interface energy between Pt and the supporting substrate is relatively high, the deposition proceeds *via* a Volmer–Weber island mechanism, where nanoparticles instead

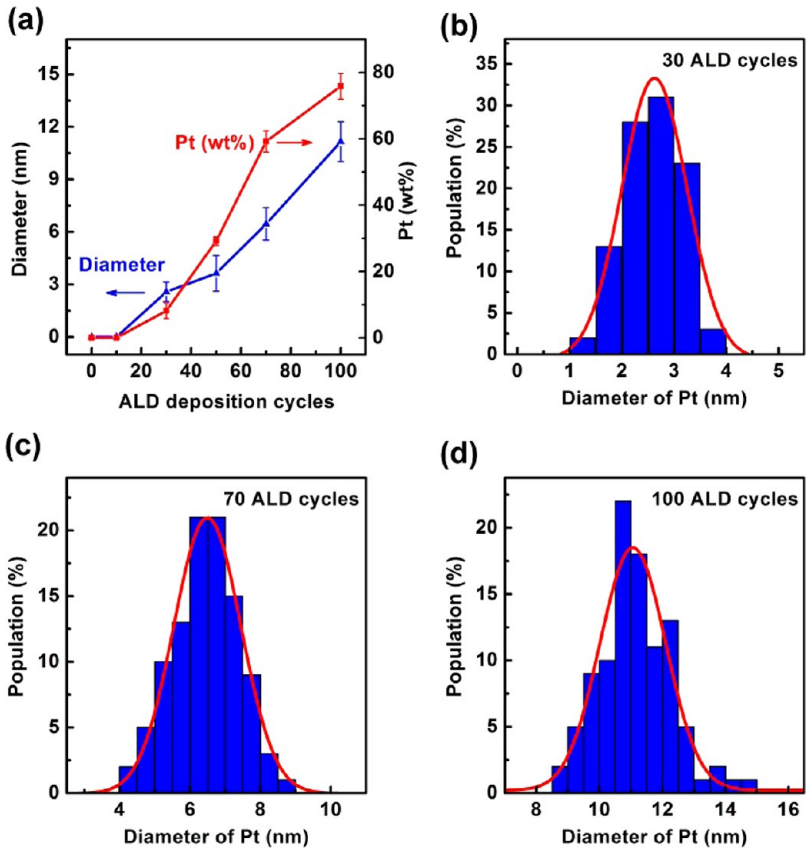

Figure 4. (a) Dependence of Pt nanoparticle sizes and mass loading (relative to the total mass of Pt and $TiSi_2$ nanonet support) on ALD cycle numbers. (b, c, d) Histograms of Pt nanoparticle diameters for 30, 70, and 100 ALD cycles of Pt deposition on $TiSi_2$ nanonets, respectively.

of uniform films are produced. With this background information in mind, we see that the deposition of Pt should favor surfaces with low energies. For C49 $TiSi_2$, theoretical studies show that *b* planes are more stable than *a* and *c* planes by up to 20% in surface energies; the difference between various planes of C54 $TiSi_2$ is much less pronounced.[25] The surface energy difference may be an important factor that governs the selective growth. It is noted that although Si-termination on the top and bottom (020) surfaces of $TiSi_2$ nanonets has been unambiguously confirmed, further research is needed to understand why no Pt particles grow on the side surfaces at all. We nonetheless emphasize that the selective deposition is highly reproducible. Moreover, it is important to note that the selectivity appears specific to Pt deposition only. For instance, ALD growth of TiO_2,[24] WO_3,[26] and Fe_2O_3[27] on $TiSi_2$ nanonets all resulted in uniform coating with no measurable dependences on the crystal planes of C49 $TiSi_2$. Lastly, we note that Pt deposition on Si nanowires was also uniform but nonselective (Figure 3e and f), ruling out the possibility that Si-termination on the $TiSi_2$ nanonet is the sole reason for the observed selectivity.

The size of Pt nanoparticles and their mass loading density were found to depend on the ALD cycles following a pseudolinear relation (Figures 4 and 2c). There was an induction time (*ca.* 10 cycles) for Pt deposition with an island nucleation on the $TiSi_2$ nanonet substrate. The sizes and mass loading of Pt increased with increasing ALD Pt cycle numbers. For 30, 50, 70, and 100 cycles of ALD Pt deposition, the mean particle sizes were 2.6 ± 0.6, 3.6 ± 1.0, 6.4 ± 0.9, and 11.2 ± 1.1 nm, respectively, and their mass loadings as determined by energy dispersive spectroscopy (EDS) were $8.2 \pm 2.3\%$, $29.2 \pm 1.3\%$, $59.2 \pm 3.2\%$, and $75.8 \pm 3.9\%$, respectively. The quantification of Pt loading was confirmed by ICP-OES (Perkin-Elmer Optima 3000 xl ICP-OES spectrometer) measurements, too.

The resulting Pt nanoparticles are crystalline in nature, as shown in Figure 5. Significantly, high-resolution TEM (HRTEM) studies revealed that more than 90% of the Pt nanoparticles grown on $TiSi_2$ nanonets exhibited a multitwinned structure. A representative example with zone axis ⟨110⟩ is shown in Figure 5a. The angles between the twin planes range from 70° to 74°, in close resemblance to other 5-fold-twinned metal nanoparticles such as Ag[28] and Au.[29] Because such twinning effect exposes Pt {111} surfaces, which are believed to be catalytically more active, research efforts have been attracted to emulate the effect by, for example, growing a Pt epitaxial overlayer[30] on multiple-twinned nanoparticle cores or alloying with Pd.[31]

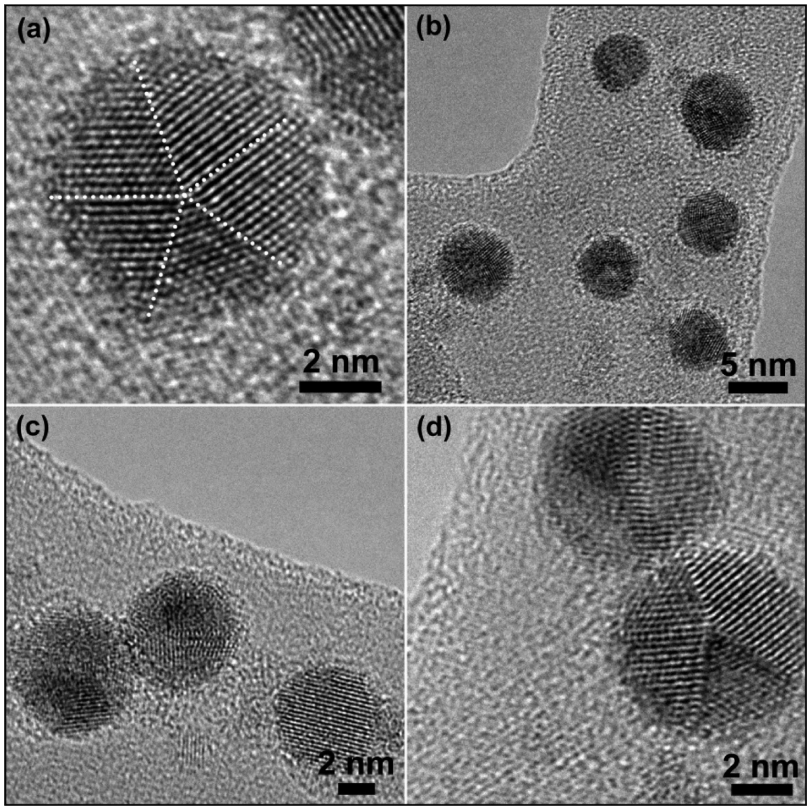

Figure 5. Representative high-magnification TEM images of multiple-twinned Pt nanoparticles deposited on $TiSi_2$ by ALD. (a) An unusual 5-fold twinning effect is observed in the high-resolution TEM image with zone axis ⟨110⟩. (b–d) High yield of multiple-twinned Pt nanoparticles.

High yields of pure Pt nanoparticles that are 5-fold twinned have not been reported previously, to the best of our knowledge. The nanonet substrate was of critical importance to the high yield of the twinned Pt nanoparticles. When the nanonet was replaced by $TiSi_2$ nanowires or TiO_2-coated nanonets, the yield of twinned Pt nanoparticles dropped dramatically to <5%, although the total number of particles deposited remained comparable. We suggest that the interaction between Pt and the $TiSi_2$ nanonet *b* planes may be the key to the formation of twinned Pt nanoparticles. Lastly, it is noted that, probably due to their small sizes, no twinned particles were observed for Pt nanoparticles smaller than 2 nm.

In an effort to benchmark the performance of the unique $TiSi_2$ nanonet–Pt nanoparticle combination, we next studied its catalytic activity for ORR in aqueous solution, in Figure 6. For comparison, electrodes of both Pt/$TiSi_2$ heteronanostructures and commercially obtained Pt/C (46 wt % supported by Vulcan carbon, Tanaka Kikinzoku) are shown in Figure 6a and b, respectively. Since the average diameter of Pt nanoparticles in the Pt/C catalyst was ~3.5 nm measured from TEM images (3–4 nm provided by vendor), we chose to test Pt nanoparticles of similar sizes, which were produced by a 50-cycle ALD growth. When $TiSi_2$ on Ti foil was used as a substrate (see Experimental Section for more details), an areal density of 50 μg_{Pt} cm_{disk}^{-2} was obtained. Note that this loading density is modest and can be readily improved if needed for future work. For example, we see much room for improvement in terms of $TiSi_2$ density and the ALD growth of Pt. Nevertheless, as a proof-of-concept and to provide a direct comparison with the Pt/$TiSi_2$ sample, the Pt/C electrode was prepared such that a comparable areal density of Pt (50 μg_{Pt} cm_{disk}^{-2}) was achieved.

Cyclic voltammetry (CV) of both $TiSi_2$/Pt and Pt/C was first obtained in 0.1 M KOH at 25 °C, and the purpose was to measure their electrochemically active surface area (ESA). We note that this group of data was collected in alkaline solutions because our later characterizations were performed in solutions of the same conditions. As shown in Figure 6c, Pt/$TiSi_2$ heteronanostructures showed CV features characteristic of Pt (111) surfaces (more detailed analysis and discussion are available in the Supporting Information), which is in excellent agreement with our HRTEM characterizations. By comparison, the CV features of Pt/C were consistent with those of Pt (110) and (100) surfaces. From this group of data, a Pt ESA of 27.9 $m^2 g^{-1}$ was obtained on Pt/C, while Pt/$TiSi_2$ exhibited a slightly higher value of 35.1 $m^2 g^{-1}$. Note that the areal densities in terms of Pt mass loading for both were comparable (*ca.* 50 μg_{Pt} cm_{disk}^{-2}). As such, the ESA difference is significant. One cause contributing to this difference may come from the multiple-twinned nature of Pt in Pt/$TiSi_2$,

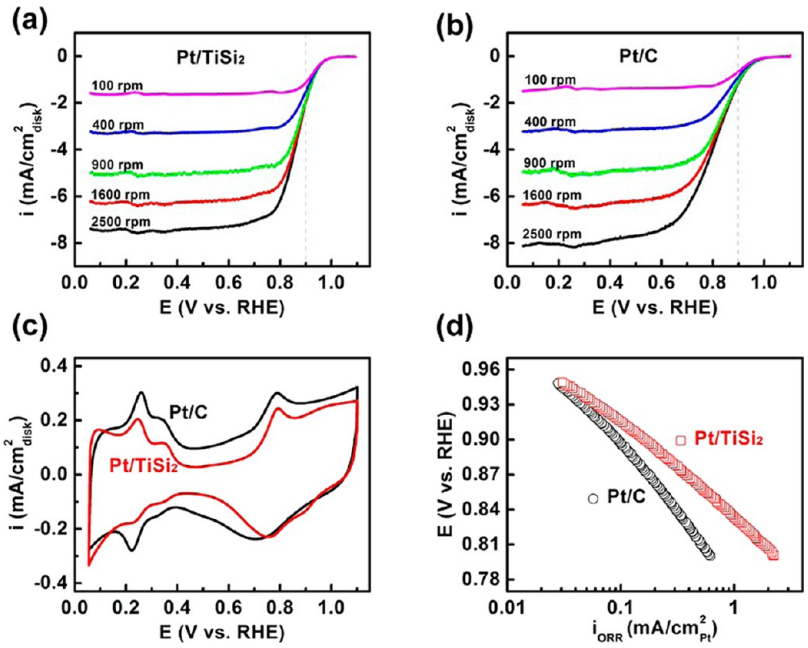

Figure 6. ORR catalytic activities of $Pt/TiSi_2$ and Pt/C in 0.1 M KOH electrolyte. (a) Polarization curves of $Pt/TiSi_2$ at a scan rate of 10 mV s^{-1} at varying rotation rates. (b) Polarization curves of Pt/C at a scan rate of 10 mV s^{-1} at various rotation rates. (c) The resulting $Pt/TiSi_2$ heteronanostructures exhibit different cyclic voltammetry characteristics (red trace) from that of a commercial Pt/C catalyst (black trace) when measured in O_2-free environments. (d) Tafel plots of the specific ORR activity of $Pt/TiSi_2$ and Pt/C based on $1/i = 1/i_k + 1/i_D$ at a rotation rate of 1600 rpm and a scan rate of 10 mV s^{-1}.

which exposes more (111) surface atoms.[30] Another reason may be found in the relatively simple interface between $Pt/TiSi_2$, which ensures more Pt exposure; by comparison, in the Pt/C mixture, carbon may wrap around Pt to reduce the effective surface areas.

To study the ORR catalytic activity, we carried out the measurements in O_2-saturated alkaline solution (0.1 M KOH, 25 °C) by the rotating disk electrode technique. ORR polarization curves of both $Pt/TiSi_2$ and Pt/C at all rotating rates showed a diffusion- or mass-transfer-controlled region at voltages below 0.6−0.7 V *vs* RHE (reversible hydrogen electrode) and diffusion−kinetic combined region above 0.7−0.8 V *vs* RHE. The limiting currents at the diffusion-controlled region are well defined as the current densities increase with $\omega^{1/2}$. As we clearly observe from Figure 6a and b, the polarization curves of $Pt/TiSi_2$ showed slight anodic shifts and more steep slopes than those of Pt/C, which indicated a better catalytic activity. The true kinetic current densities shown in Figure 6d were calculated according to the Koutecky−Levich equation (see Supporting Information). A nonoptimized $Pt/TiSi_2$ combination already exhibited superior performance when compared with the optimized commercial Pt/C. At 0.9 V *vs* RHE, the corrected kinetic current density of the $Pt/TiSi_2$ heteronanostructure was 160 μA cm^2_{Pt}, which is considerably higher than 90 μA cm^2_{Pt} of Pt/C, indicating much higher ORR activity for the selectively grown Pt on $TiSi_2$ nanonets (see Supporting Information for discussions about how these values compare with literature reports). We suggest that the 5-fold twinned nature of the Pt nanoparticles is an important reason for the performance difference. We also noticed that $Pt/TiSi_2$ and Pt/C samples had slightly different slopes of 80.2 and 110.9 mV/decade, respectively, which is again in good agreement with literature reports of pure Pt (111) and Pt (100) surfaces in 0.1 M KOH.[32]

To optimize the properties of $Pt/TiSi_2$ for further improvement of the catalytic activities as shown in Figure 6, we envision that the charge transfer kinetics may be increased by further optimizing the ALD process. In addition, we also predict that if the gas diffusion is improved, the saturation current should increase, as well. To reduce the limitation of mass transfer, we next show a set of experiments we carried out on porous supporting charge collectors of Ti mesh. Since $TiSi_2$ nanonets can be synthesized on a variety of different substrates,[17] this idea was readily tested. As a proof-of-concept, we chose to grow $TiSi_2$ nanonets on Ti mesh (wire diameter 250 μm; pore size 200 μm; Cleveland Wire Cloth), followed by ALD deposition of Pt nanoparticles. Structural studies by scanning electron microscopy (SEM) revealed that $TiSi_2$ nanonets grew uniformly on Ti mesh (Figure 7a), including the junction areas of the interwoven wires (Figure 7b). A higher magnification scanning electron micrograph as shown in Figure 7c confirmed that $TiSi_2$ nanonets were of high density and purity. A significant advantage of the $TiSi_2$ nanonet synthesis is that the growth does not require growth catalysts, which greatly simplifies the electrode fabrication process and avoids producing

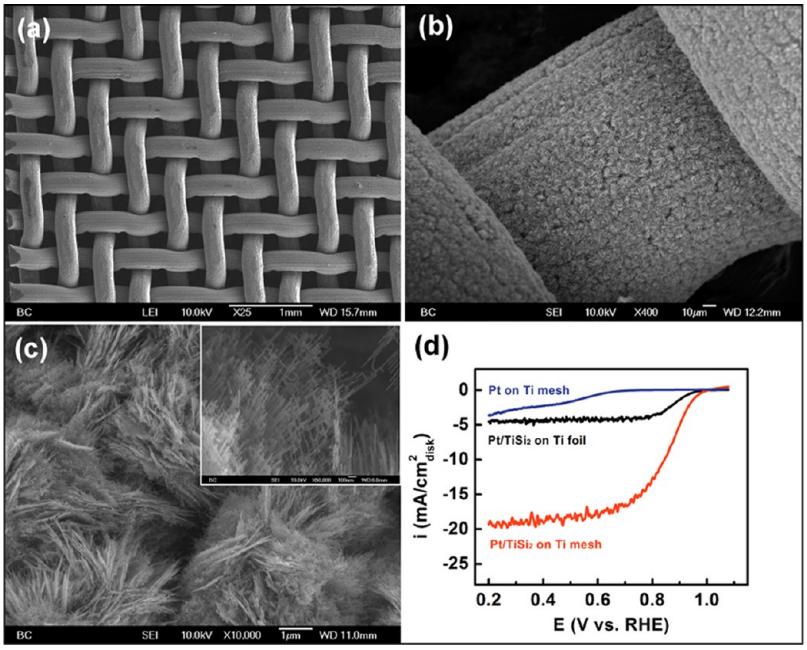

Figure 7. Structures of Pt/$TiSi_2$ heteronanostructures prepared on Ti mesh and their catalytic activities. (a–c) Low-, medium-, and high-magnification SEM images of Pt/$TiSi_2$ grown on Ti mesh. Inset in (c): a 50 000× magnified view to reveal the two-dimensional nature of the nanonet morphology. (d) Polarization curve for ORR of Pt/$TiSi_2$ on mesh in 0.1 M KOH at a scan rate of 20 mV s^{-1} at 25 °C. As a comparison, the performances of Pt on Ti mesh in the absence of $TiSi_2$ nanonets (blue trace) and Pt/$TiSi_2$ on Ti foil (black trace) are shown. The Pt loading on $TiSi_2$ coated Ti foil and Ti mesh sample are 50 and 99 μg_{Pt} cm_{geo}^{-2}, respectively.

unnecessary impurities to undermine the catalytic activities.

Importantly, a saturation current density of 19.3 mA cm_{geo}^{-2} was measured (Figure 7d), which represents an almost 3-fold increase as compared with $TiSi_2$ on planar Ti foil. Note that the Pt loading per unit geometric area increased only from 50 to 99 μg_{Pt} cm_{geo}^{-2}, corresponding to an increase of only 1-fold. We therefore understand the greater current density of Ti mesh samples as a result of better O_2 diffusion but not a simple increase of Pt loading. In general, the saturation current density in an ORR reaction is limited by three factors: the resistance in charge transfer, the resistance in charge transport, and the limitation of mass transport. Because the nature of Pt nanoparticles grown on $TiSi_2$/Ti mesh is identical to that of Pt nanoparticles prepared on $TiSi_2$/Ti foil, the differences in charge transfer and transport are expected to be negligible. As such, the change in mass transfer is the most plausible reason to explain the observed enhancement of saturation current densities. Similar results have been observed on traditional carbon paper when acting as a gas diffusion layer to enhance the mass transfer of O_2.[33] In addition, metal foams and meshes have been applied as Pt supports as well, especially in the case of direct methanol fuel cells.[34,35]

CONCLUSIONS

In conclusion, we have demonstrated a highly selective Pt growth on the *b* planes of $TiSi_2$ nanonets by atomic layer deposition. As-grown Pt nanoparticles exhibited an unusual 5-fold twinned structure that preferably exposes {111} surfaces of Pt. Because the resulting material showed high activity toward ORR reactions, it has great potential as a promising air cathode for applications such as proton exchange membrane fuel cells. The availability of non-carbon electrode construction, such as the Pt/$TiSi_2$ combination reported here, adds value in that it permits fundamental studies to discern what role carbon support plays in existing devices. In addition, these open structures may prove effective in enabling high current densities, which is a highly coveted feature for applications such as electric transportation.

EXPERIMENTAL SECTION

$TiSi_2$ Nanonet Synthesis. $TiSi_2$ nanonets were synthesized by a chemical vapor deposition method. A Ti foil (Sigma-Aldrich, 0.127 mm thick, purity 99.7%) was placed in a home-built reaction chamber and heated to 675 °C. Then, SiH_4 (10% in He, Voltaix; at 50 standard cubic centimeters per minute, or sccm), $TiCl_4$ (98%, Sigma-Aldrich; 2 sccm), and H_2 (industrial grade, Airgas; 60 sccm) were introduced to the chamber, and the pressure was maintained constant at 5 Torr. The growth duration was typically 10–120 min for varying sizes and densities of nanonets.

TiO_2-Coated $TiSi_2$ Nanonets. TiO_2 was deposited in a Cambridge Nanotech (Savannah 100) ALD system following procedures we previously reported.[24] In brief, the reaction took place at 275 °C with a constant flow of N_2 at 20 sccm. Titanium(IV) isopropoxide ($Ti(^iPrO)_4$, heated to 75 °C) and deionized H_2O (room temperature)

were used as reaction precursors. The pulse and purge times for $Ti(^iPrO)_4$ and H_2O were 50 ms and 10 s, 15 ms and 10 s, respectively. A 10-cycle growth of TiO_2 (estimated thickness 0.5 nm) was applied to the $TiSi_2$ nanonets to modify the surface.

Si Nanowires. The preparation of Si NWs was reported previously.[36] Briefly, the Si (100) substrate (Wafernet) was cleaned with acetone, methanol, and 2-propanol sequentially. The substrate was then oxidized in H_2O_2/H_2SO_4 (1:3 vol/vol) solution at 90 °C for 10 min to remove heavy metals and organic residue and then rinsed by deionized water. Finally, the cleaned substrate was immersed into an $HF/AgNO_3$ solution (4 M HF and 0.02 M $AgNO_3$) for 30 min at 50 °C to produce Si NWs.

Atomic Layer Deposition of Pt. Pt nanoparticles were deposited in an Arradiance (Gemstar) atomic layer deposition system. The growth temperature was 250 °C, with trimethyl-methylcyclopentadienyl platinum(IV) ($MeCpPtMe_3$, heated to 75 °C) and compressed air (room temperature) as reaction precursors. Each cycle consisted of four repeated pulse/purges of $MeCpPtMe_3$ for sufficient surface adsorption and one pulse/purge of O_2 to decompose $MeCpPtMe_3$. The purge gas was N_2, and its flow rate was 90 sccm.

Material Characterizations. As-grown samples were imaged using a transmission electron microscope (JEOL 2010F) and a scanning electron microscope (JEOL 6340F). The TEM was operated at an acceleration voltage of 200 kV, and the SEM was at 10 kV. Elemental analysis was conducted using an EDS attachment to the TEM.

Electrochemical Characterizations. $Pt/TiSi_2$ on flat Ti foil was attached onto the rotating disk electrode (glassy carbon electrode, 5 mm in diameter, Pine Instrument Co.) for electrochemical measurements. The Pt/C electrode in the control experiment was prepared by first ultrasonicating the Pt/C nanoparticles (46 wt % supported by Vulcan carbon, Tanaka Kikinzoku, average diameter of Pt nanoparticles is 3.5 nm) in deionized water (Millipore, 18.2 MΩ) for 1 h to make the ink and then drop-casting the catalyst ink onto the same type of rotating disk electrode. The loading of nanoparticles was 50 $\mu g_{Pt}/cm^2_{disk}$.

Measurement of Effective Surface Area. Cyclic voltammograms were collected in 0.1 M KOH solutions at a temperature maintained at 25 °C. A Pt wire sealed in glass tubing and an Ag/AgCl electrode (4 M KCl, Pine Instrument Co.) were used as counter and reference electrode, respectively. The electrolyte was purged with N_2 (ultrahigh purity, Airgas) for 30 min before measurements. CVs were recorded at a scan rate of 50 mV s^{-1} between 0.05 and 1.10 V *vs* RHE until they were stabilized. CVs were then recorded and presented at a scan rate of 10 mV s^{-1} in the same voltage range for ESA measurements.

Characterization of Oxygen Reduction Activities. After ESA measurements, electrolyte was purged with O_2 (ultrahigh purity, Airgas) for 30 min before evaluating ORR activities of $Pt/TiSi_2$ and Pt/C samples. Polarization curves were recorded at various rotating rates (2500, 1600, 900, 400, 100 rpm) at a scan rate of 10 mV s^{-1} between 0.05 and 1.10 V *vs* RHE. To correct for capacitance contribution, oxygen reduction currents were obtained by subtracting the polarization curve in N_2 from the corresponding curve in O_2.

Conflict of Interest: The authors declare no competing financial interest.

Supporting Information Available: Effective surface area measurements and discussions about ORR activities. This material is available free of charge *via* the Internet at http://pubs.acs.org.

Acknowledgment. This work is supported by Boston College and in part by the National Science Foundation (DMR 1055762). D. Wang is an Alfred P. Sloan Fellow. We thank S. Shepard and Dr. D. Wang for technical assistance and Dr. C.-H. Kuo and Prof. C.-K. Tsung for insightful discussions. We also thank Dr. D. Zheng at UMass Boston for elemental analysis.

REFERENCES AND NOTES

1. Bruce, P.; Scrosati, B.; Tarascon, J. M. Nanomaterials for Rechargeable Lithium Batteries. *Angew. Chem., Int. Ed.* **2008**, *47*, 2930–2946.
2. Goodenough, J. B.; Kim, Y. Challenges for Rechargeable Li Batteries. *Chem. Mater.* **2010**, *22*, 587–603.
3. Yang, P.; Tarascon, J. M. Towards Systems Materials Engineering. *Nat. Mater.* **2012**, *11*, 560–563.
4. Markovic, N. M.; Schmidt, T. J.; Stamenkovic, V.; Ross, P. N. Oxygen Reduction Reaction on Pt and Pt Bimetallic Surfaces: A Selective Review. *Fuel Cells* **2001**, *1*, 105–116.
5. Gasteiger, H. A.; Kocha, S. S.; Sompalli, B.; Wagner, F. T. Activity Benchmarks and Requirements for Pt, Pt-alloy, and Non-Pt Oxygen Reduction Catalysts for PEMFCs. *Appl. Catal., B* **2005**, *56*, 9–35.
6. Stamenkovic, V. R.; Fowler, B.; Mun, B. S.; Wang, G.; Ross, P. N.; Lucas, C. A.; Markovic, N. M. Improved Oxygen Reduction Activity on $Pt_3Ni(111)$ *via* Increased Surface Site Availability. *Science* **2007**, *315*, 493–497.
7. Gasteiger, H. A.; Markovic, N. M. Just a Dream-or Future Reality? *Science* **2009**, *324*, 48–49.
8. Stephens, I. E. L.; Bondarenko, A. S.; Perez-Alonso, F. J.; Calle-Vallejo, F.; Bech, L.; Johansson, T. P.; Jepsen, A. K.; Frydendal, R.; Knudsen, B. P.; Rossmeisl, J.; *et al*. Tuning the Activity of Pt(111) for Oxygen Electroreduction by Subsurface Alloying. *J. Am. Chem. Soc.* **2011**, *133*, 5485–5491.
9. Wang, J.; Yin, G.; Shao, Y.; Zhang, S.; Wang, Z.; Gao, Y. Effect of Carbon Black Support Corrosion on the Durability of Pt/C Catalyst. *J. Power Sources* **2007**, *171*, 331–339.
10. Adzic, R. R.; Zhang, J.; Sasaki, K.; Vukmirovic, M. B.; Shao, M.; Wang, J. X.; Nilekar, A. U.; Mavrikakis, M.; Valerio, J. A.; Uribe, F. Platinum Monolayer Fuel Cell Electrocatalysts. *Top. Catal.* **2007**, *46*, 249–262.
11. Stamenkovic, V. R.; Mun, B. S.; Arenz, M.; Mayrhofer, K. J. J.; Lucas, C. A.; Wang, G.; Ross, P. N.; Markovic, N. M. Trends in Electrocatalysis on Extended and Nanoscale Pt-Bimetallic Alloy Surfaces. *Nat. Mater.* **2007**, *6*, 241–247.
12. Strasser, P.; Koh, S.; Anniyev, T.; Greeley, J.; More, K.; Yu, C.; Liu, Z.; Kaya, S.; Nordlund, D.; Ogasawara, H.; *et al*. Lattice-Strain Control of the Activity in Dealloyed Core-Shell Fuel Cell Catalysts. *Nat. Chem.* **2010**, *2*, 454–460.
13. Ding, Y.; Kim, Y. J.; Erlebacher, J. Nanoporous Gold Leaf: "Ancient Technology"/Advanced Material. *Adv. Mater.* **2004**, *16*, 1897–1900.
14. Peng, Z.; Freunberger, S. A.; Chen, Y.; Bruce, P. G. A Reversible and Higher-Rate Li-O_2 Battery. *Science* **2012**, *337*, 563–566.
15. Zhou, S.; Liu, X.; Lin, Y.; Wang, D. Spontaneous Growth of Highly Conductive Two-Dimensional Single-Crystalline $TiSi_2$ Nanonets. *Angew. Chem., Int. Ed.* **2008**, *47*, 7681–7684.
16. Zhou, S.; Liu, X.; Lin, Y.; Wang, D. Rational Synthesis and Structural Characterizations of Complex $TiSi_2$ Nanostructures. *Chem. Mater.* **2009**, *21*, 1023–1027.
17. Zhou, S.; Xie, J.; Wang, D. Understanding the Growth Mechanism of Titanium Disilicide Nanonets. *ACS Nano* **2011**, *5*, 4205–4210.
18. Zhou, Z.-Y.; Tian, N.; Li, J.-T.; Broadwell, I.; Sun, S.-G. Nanomaterials of High Surface Energy with Exceptional Properties in Catalysis and Energy Storage. *Chem. Soc. Rev.* **2011**, *40*, 4167–4185.
19. Bing, Y.; Liu, H.; Zhang, L.; Ghosh, D.; Zhang, J. Nanostructured Pt-Alloy Electrocatalysts for PEM Fuel Cell Oxygen Reduction Reaction. *Chem. Soc. Rev.* **2010**, *39*, 2184–2202.
20. Christensen, S. T.; Elam, J. W.; Rabuffetti, F. A.; Ma, Q.; Weigand, S. J.; Lee, B.; Seifert, S.; Stair, P. C.; Poeppelmeier, K. R.; Hersam, M. C.; Bedzyk, M. J. Controlled Growth of Platinum Nanoparticles on Strontium Titanate Nanocubes by Atomic Layer Deposition. *Small* **2009**, *5*, 750–757.
21. Pacholski, C.; Kornowski, A.; Weller, H. Site-Specific Photodeposition of Silver on ZnO Nanorods. *Angew. Chem., Int. Ed.* **2004**, *43*, 4774–4777.
22. Habas, S. E.; Yang, P. D.; Mokari, T. Selective Growth of Metal and Binary Metal Tips on CdS Nanorods. *J. Am. Chem. Soc.* **2008**, *130*, 3294–3295.
23. Amirav, L.; Alivisatos, A. P. Photocatalytic Hydrogen Production with Tunable Nanorod Heterostructures. *J. Phys. Chem. Lett.* **2010**, *1*, 1051–1054.

24. Lin, Y.; Zhou, S.; Liu, X.; Sheehan, S.; Wang, D. TiO_2/$TiSi_2$ Heterostructures for High-Efficiency Photoelectrochemical H_2O Splitting. *J. Am. Chem. Soc.* **2009**, *131*, 2772–2773.
25. Wang, T.; Oh, S.-Y.; Lee, W.-J.; Kim, Y.-J.; Lee, H.-D. Ab Initio Comparative Study of C54 and C49 $TiSi_2$ Surfaces. *Appl. Surf. Sci.* **2006**, *252*, 4943–4950.
26. Liu, R.; Lin, Y.; Chou, L.-Y.; Sheehan, S. W.; He, W.; Zhang, F.; Hou, H. J. M.; Wang, D. Water Splitting by Tungsten Oxide Prepared by Atomic Layer Deposition and Decorated with an Oxygen-Evolving Catalyst. *Angew. Chem., Int. Ed.* **2011**, *50*, 499–502.
27. Lin, Y.; Zhou, S.; Sheehan, S. W.; Wang, D. Nanonet-Based Hematite Heteronanostructures for Efficient Solar Water Splitting. *J. Am. Chem. Soc.* **2011**, *133*, 2398–2401.
28. Sun, Y.; Ren, Y.; Liu, Y.; Wen, J.; Okasinski, J. S.; Miller, D. J. Ambient-Stable Tetragonal Phase in Silver Nanostructures. *Nat. Commun.* **2012**, *3*, 971.
29. Sanchez-Iglesias, A.; Pastoriza-Santos, I.; Perez-Juste, J.; Rodriguez-Gonzalez, B.; de Abajo, F. J. G.; Liz-Marzan, L. M. Synthesis and Optical Properties of Gold Nanodecahedra with Size Control. *Adv. Mater.* **2006**, *18*, 2529–2534.
30. Yang, J.; Yang, J.; Ying, J. Y. Morphology and Lateral Strain Control of Pt Nanoparticles *via* Core−Shell Construction Using Alloy AgPd Core toward Oxygen Reduction Reaction. *ACS Nano* **2012**, *6*, 9373–9382.
31. Xia, Y. N.; Xiong, Y. J.; Lim, B.; Skrabalak, S. E. Shape-Controlled Synthesis of Metal Nanocrystals: Simple Chemistry Meets Complex Physics? *Angew. Chem., Int. Ed.* **2009**, *48*, 60–103.
32. Ross, P. N. Oxygen Reduction Reaction on Smooth Single Crystal Electrodes. In *Handbook of Fuel Cells*; John Wiley & Sons, Ltd: New York, 2010.
33. Liang, Y.; Li, Y.; Wang, H.; Zhou, J.; Wang, J.; Regier, T.; Dai, H. Co_3O_4 Nanocrystals on Graphene as a Synergistic Catalyst for Oxygen Reduction Reaction. *Nat. Mater.* **2011**, *10*, 780–786.
34. Arisetty, S.; Prasad, A. K.; Advani, S. G. Metal Foams as Flow Field and Gas Diffusion Layer in Direct Methanol Fuel Cells. *J. Power Sources* **2007**, *165*, 49–57.
35. Chen, R.; Zhao, T. S. A Novel Electrode Architecture for Passive Direct Methanol Fuel Cells. *Electrochem. Commun.* **2007**, *9*, 718–724.
36. Yuan, G. B.; Aruda, K.; Zhou, S.; Levine, A.; Xie, J.; Wang, D. W. Understanding the Origin of the Low Performance of Chemically Grown Silicon Nanowires for Solar Energy Conversion. *Angew. Chem., Int. Ed.* **2011**, *50*, 2334–2338.